

CONF-961111-1  
ANL/ITD/CP-91635

Explosives Detection Studies Using Fast-Neutron Transmission Spectroscopy

RECEIVED  
DEC 16 1996  
OSTI

C. L. Fink, B. J. Micklich, L. Sagalovsky, D. L. Smith, and T. J. Yule

Technology Development Division  
Argonne National Laboratory  
9700 South Cass Avenue, Argonne, IL 60439 USA

### ABSTRACT

Fast-Neutron Transmission Spectroscopy (FNTS) is being investigated for detection of explosives in luggage or air cargo. We present here the principle results of a two-year study of a few-view tomographic FNTS system using the Monte Carlo radiation transport code MCNP to simulate neutron transmission through simple luggage phantoms and Receiver Operator Characteristic (ROC) curves to determine system performance. Elemental distributions along projections through the interrogated object are obtained by analyzing MCNP generated neutron transmission data. Transmission data for few (3-5) angles and relatively coarse resolution ( $\sim 2$  cm) are used to create a tomographic reconstruction of elemental distributions within the object. The elemental unfolding and tomographic reconstruction algorithms and the concept of transmission-derived cross sections for use in elemental analysis have been validated by application to experimental data. Elemental distributions are combined in an explosives detection algorithm to provide an indication of the presence or absence of explosives. The algorithm in current use, termed the "equivalent explosive" algorithm, determines the quantity of explosive that can be formed using the measured amount of the constituent elements in each pixel. Reconstruction and explosives detection algorithms have been applied to a series of randomly packed suitcases to generated ROC that describe system performance in terms of the probability of detection and of false alarms. System studies have been performed to study the operational characteristics and limitations of a FNTS system, and to determine the system's sensitivity to several important parameters such as neutron source reaction and incident particle energy, flight path length, and the position of the interrogated object.

### 1. Overview

This paper provides a summary of the key results from model studies of a Fast-Neutron Transmission Spectroscopy (FNTS) system that uses few-view tomography and relatively coarse detector resolution. The model was developed as part of a two-year FAA effort [1] designed to provide realistic assessment of the key issues involved in using FNTS for explosive detection and has been verified, where possible, using experimental data. An important advantage of modeling an FNTS system is that it permits variations in system design, algorithms, and parameters to be studied with minimal cost and in relatively short periods of time. The model was also used with a random suitcase packing algorithm to produce Receiver Operator Characteristic (ROC) curves [2] that characterize system performance. The use of ROC curves is important because the interaction of the various model components are nonlinear and it is difficult to determine the effect of a change in a single model component or parameter on system performance. We also present some results from system studies on issues related to the design and implementation of a FNTS system in an airport environment.

### 2. Description of the FNTS Concept

MASTER

The FNTS technique is one of several neutron interrogation methods being examined for detection of illicit substances such as explosives and narcotics. The use of fast neutrons is attractive because, unlike x-ray transmission, neutron transmission is more sensitive to the presence of the light elements hydrogen, carbon, nitrogen, and oxygen. Explosives are composed primarily of these elements, but are relatively rich in nitrogen and oxygen and relatively poor in carbon compared to most benign substances likely to be found in luggage or cargo. The FNTS technique was first used by Overly [3] to determine compositions of bulk organic materials, and is best suited for examination of luggage or small containers having an energy-averaged transmission ratio greater than about 0.01. The technique uses an accelerator to produce nanosecond pulsed beams of protons or deuterons which strike a target and produce a pulsed beam of neutrons with a continuum of energies. The interrogated material is placed in the flight path between the accelerator target and the neutron detector array. Time-of-flight techniques are used to measure the neutron

## **DISCLAIMER**

This report was prepared as an account of work sponsored by an agency of the United States Government. Neither the United States Government nor any agency thereof, nor any of their employees, makes any warranty, express or implied, or assumes any legal liability or responsibility for the accuracy, completeness, or usefulness of any information, apparatus, product, or process disclosed, or represents that its use would not infringe privately owned rights. Reference herein to any specific commercial product, process, or service by trade name, trademark, manufacturer, or otherwise does not necessarily constitute or imply its endorsement, recommendation, or favoring by the United States Government or any agency thereof. The views and opinions of authors expressed herein do not necessarily state or reflect those of the United States Government or any agency thereof.

## **DISCLAIMER**

**Portions of this document may be illegible  
in electronic image products. Images are  
produced from the best available original  
document.**

transmission through the sample as a function of neutron energy. Since the neutron total cross section for light elements varies widely in the measured neutron energy range, the transmission spectrum depends on the integrated density of the elements present in the line-of-sight from the neutron source to the detector and on the total cross sections of those elements. The individual elemental areal densities (atoms per  $\text{cm}^2$ ) are obtained by a linear least-squares unfolding of the transmission spectrum using the total cross sections for the elements of interest [4].

Clearly it would be preferable from a system point of view to use the elemental areal densities to obtain radiographic images of the suitcase for each of the elements of interest and then combine these results in such a way as to obtain an image that indicates the presence or absence of an explosive. The problem is that overlap of elemental densities from different objects along the projection path leads to false negatives (failure to detect explosives/drugs when present) and false positives (indication of explosives/drugs when not actually present). To reduce this overlap it is possible to use tomographic reconstruction techniques not unlike those used by tomographic x-ray systems. For neutron systems, however, the number of projections will be limited to 3 to 7 and the pixel resolutions will be limited to 1-3 cm because of constraints in inspection time and detector cost.

### 3. FNTS System Model

A tomographic FNTS inspection system requires four distinct steps to arrive at a decision on the presence or absence of an explosive in luggage [5]. These are (1) the unfolding of the elemental projection density information from the transmission data, (2) the tomographic reconstruction of the elemental density distributions within the suitcase, (3) the combination of the elemental density distributions into an explosive signature that maximizes sensitivity to the explosive and minimizes sensitivity to background objects, and (4) the use of an image processing algorithm to separate the explosive signature from background noise.

#### *Elemental Unfolding of Transmission Data*

A key issue in FNTS is the ability of the elemental unfolding algorithm to accurately unfold elemental densities from experimental transmission data. We have looked at two situations. In the first we used the radiation transport code MCNP [6] to calculate the transmissions for typical phantoms and then compared the unfolded areal densities with those of the actual phantom. In general, we found good agreement except for the case in which two objects of dissimilar densities fill a pixel. This case is shown in Figure 1, which shows a single projection transmission channel aligned with the major axis of a sheet explosive. The response seen by the detector is a sum of the transmission through the nonexplosive portion of the projection bin  $T_s$  and the explosive portion  $T_e$ . The elemental response determined from the detector data will be an average of the material in the nonexplosive portion of the projection bin and that in the explosive portion, weighted by the transmission through each of these regions. Since the transmission through the explosive region will be smaller than through the nonexplosive region, the nonexplosive material will dominate the detector response. In fact, if the transmission through the explosive is zero, then the detector response will be entirely determined by the nonexplosive region. The only observable indication of a problem would be a reduced count rate in the detector. This problem of partially filled pixels can be generalized to any case in which a single pixel contains two or more materials that present greatly different transmissions, such as an edge pixel that has a partial void. The problem is not one that is unique to edges or to internal optically thick regions, and is ultimately one of finite resolution (since smaller pixel sizes would be capable of resolving the objects contained inside a larger pixel).

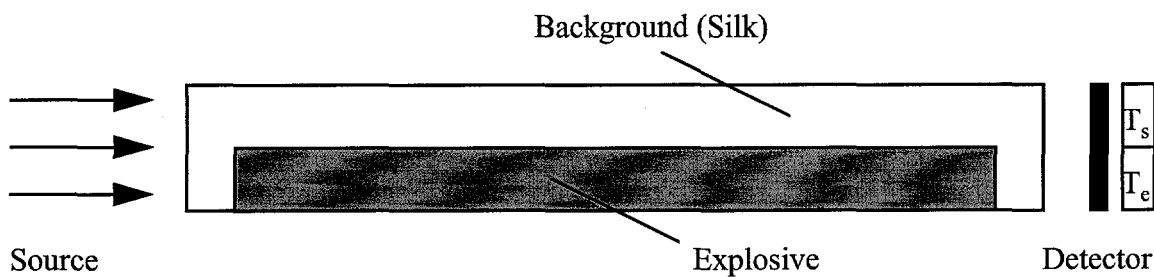


Figure 1. Geometry of a projection channel containing a thin sheet of explosive and silk.

These results clearly show the importance of performing modeling studies using codes like MCNP. The simulation correctly calculates the attenuation through a partially-filled pixel as  $\langle \exp(-\Sigma x) \rangle$ , while the ray-tracing approximation for exact quantities calculates  $\exp(-\langle \Sigma x \rangle)$ . The results also indicate that detecting thin sheets of explosives using pixel resolutions several times larger than the sheet size will be more difficult than expected.

We have also compared [7] unfolded data with actual experimental data taken by a group at the University of Oregon [8]. The transmission-derived cross sections [9] used in the unfolding were calculated using the radiation transport code MCNP for a  $^9\text{Be}(\text{d},\text{n})$  source at  $E_d = 4.2$  MeV and a 4-m flight path with the sample located midway between source and detector (these parameter values correspond to the experimental conditions). We found, for the 58 items studied, very good agreement between the areal densities obtained by Oregon using experimentally determined cross sections and the results of the present analysis using transmission-derived cross sections calculated with MCNP. The transmission-derived cross sections do have sharper features than the cross sections used by the Oregon group, and the resulting attenuation curves appear to fit the experimental data somewhat better. The good agreement seen between the experimental attenuation data and the unfolding results confirms the validity of the elemental unfolding algorithm and the use of transmission-derived cross sections for unfolding experimental data. Because of this good agreement, we have investigated the problem of the presence of other elements other than hydrogen, carbon, oxygen, and nitrogen on the unfolding accuracy using Monte Carlo derived transmission spectra. Initial studies of this effect indicate that these additional elements can have significant impact on the unfolding accuracy unless they are explicitly included in the unfolding.

#### *Tomographic Reconstruction*

Because the number of projection angles will be limited, the FNTS system uses algebraic reconstruction techniques. For this initial evaluation we have used the Maximum Likelihood Method although other reconstruction algorithms are being evaluated [10]. Because we were interested in different pixel and projection resolutions as well as nonsquare object sizes, we developed our own series of reconstruction programs using FORTRAN90. We also assumed that the suitcase would be examined in a series of square slices with the dimensions of each slice corresponding to a 60-cm square. The projection resolution was varied between 1 and 2 cm and the reconstructed pixel resolution between 1 and 3 cm.

#### *Explosive Signature*

The tomographic reconstruction provides the H, C, N, and O density distributions. These density distributions must be combined to maximize the signature from an explosive and to minimize the background signature from nonexplosive objects. The process is further complicated by the fact that a wide range of explosives must be considered. For this study we use the concept of maximum equivalent explosive signature [11]. Each pixel has a calculated H, C, N, and O density. The equivalent explosive signature for a pixel is obtained by dividing each of these measured elemental densities by the corresponding elemental mass fraction of the explosive of interest. The smallest of the four densities is the equivalent explosive density since the element yielding the smallest value limits the amount of explosive present in the pixel. If there is the possibility of several different types of explosives, we calculate an equivalent explosive density for each explosive and use the largest. Note that effectiveness of this algorithm is enhanced by the high density of explosives ( $\sim 1.6$  g/cm $^3$ ). Since we were mainly interested in studying the effect of the reconstruction algorithms, we used a single explosive (RDX) in the system evaluation. However, since any element can in principle be identified by the unfolding algorithm, explosives which are not characterized by high N and O content could also be tested for by including them in the explosive database.

#### *Image Processing Algorithm*

To detect the presence of explosives, we used a simple binary image processing algorithm in which an explosive is considered present in the image if the area of all pixels greater than some equivalent explosive density threshold is greater than some specified value [10,12]. Thus the decision variable in generating the ROC curves is a function of the threshold and the area. Clearly the image detection algorithm could be improved by also including information on the spatial distribution of the pixels above the threshold.

#### 4. Model Performance Using Experimental Data

We have applied the model described in Section 3 to multiview experimental data acquired by the University of Oregon in their transmission time-of-flight experiments [8]. A suitcase was randomly chosen from a group of lost luggage and a quantity of C-4 explosive was placed inside. The exact size and position of the explosive was unknown. The transmission measurements collected data using a linear array of sixteen detectors that viewed a slice through the suitcase. The suitcase was scanned by varying its elevation. Four scan angles of 0, 45, 90, and 135 degrees were used. The size of each detector is nominally 2.5 inches. This translates to a pixel size of approximately 3.18-cm square at the center. In general, the measured densities are low and suggest that this suitcase was relatively lightly packed. Figure 2 shows the equivalent explosive density for slices at various elevations within the suitcase. The size of each slice is 48 cm by 48 cm. The number above the reconstruction is the elevation number. Here 109 corresponds to the middle of the suitcase, and 102 corresponds to the bottom. The presence of an explosive near the bottom of the image is easily seen. The data show that the explosive size is approximately 9 to 10 cm high (approximately three slices) and approximately 6 cm (2 pixels) square. Note that the equivalent explosive density from other regions and slices is relatively small. Thus for suitcases with this packing density, the false-positive frequency should be low for large bulk explosives. Thinner explosives might require lower explosive density thresholds and could increase the false positive rate.

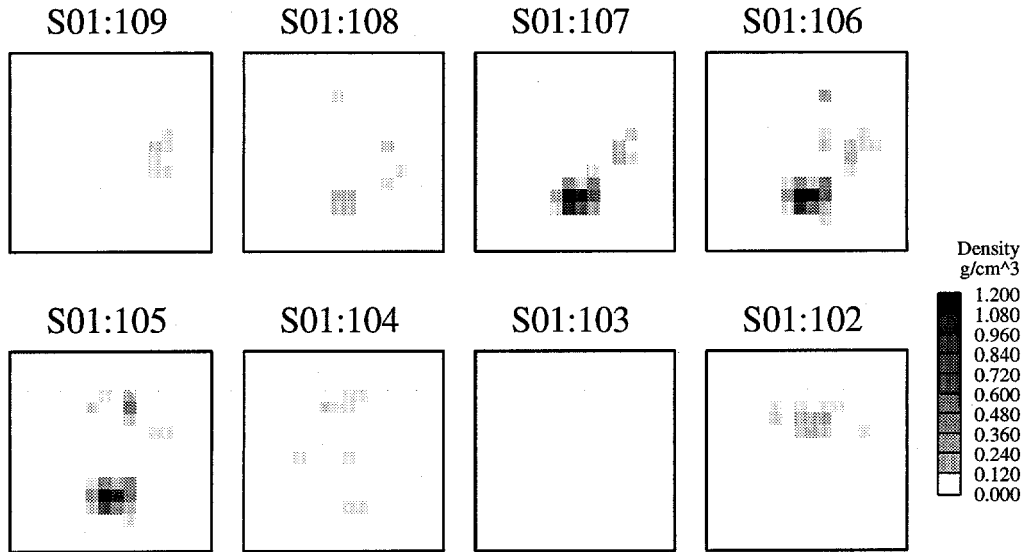


Figure 2. Equivalent explosive density vs. position for the Oregon suitcase. Pixels are approximately 3 cm square.

#### 5. Model Suitcase Studies

Because the interaction between the various components, algorithms, and parameters of the FNTS model are nonlinear it is difficult to assess changes of one parameter on another. For example, is the number of projection angles or the detector resolution more important in terms of system performance? We studied these questions by developing a simple suitcase packing algorithm and using the model of Section 3 to generate a series of ROC curves as function of system parameters [10,12]. Some of the parameters that were varied were the projection resolution, the pixel resolution, the number of projection angles, the type of reconstruction algorithm, and the explosive size and shape. In addition, we looked at how different suitcase packing schemes effected the results. For most of the studies we used an ensemble of 1000 suitcases. Figures 3 show the ROC curves obtained for the case of five projection angles and for the three different explosives shapes. Note that in this case the exact projection data were used rather than MCNP generated data. It is clear that bulk explosives can be relatively easily detected, but that thin slabs will be considerably more difficult.

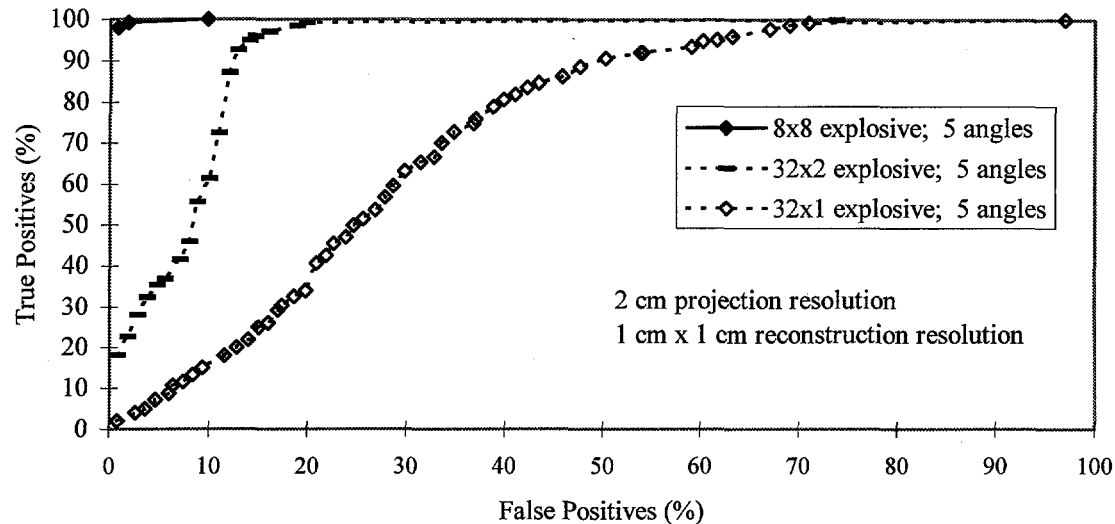


Figure 3. ROC curves for different explosive shapes.

## 6. System Studies

Systems studies are useful for exploring the sensitivity of a FNTS system to changes in parameters or engineering designs. As in the case of explosive detection algorithms, it is generally easier and less expensive to determine these sensitivities through modeling than through experiment. Studies have been conducted to examine the effect on system performance of the incident deuteron energy for the  $^9\text{Be}(\text{d},\text{n})$  source reaction, the use of the  $^9\text{Be}(\text{p},\text{n})$  reaction as an alternative source, the flight path length, and the sample position relative to the detector array.

MCNP simulations were performed to determine the elemental unfolding errors as functions of projectile energy in the  $^9\text{Be}(\text{d},\text{n})$  reaction. For deuteron energies greater than 4.2 MeV, errors are smaller because the source contains a significant number of neutrons up to 3.2 MeV, which corresponds to the energy of a prominent cross section resonance in carbon. There exists, however, a high-energy tail which contributes little information but constitutes a shielding problem. The  $^9\text{Be}(\text{p},\text{n})$  reaction with  $E_p = 5$  MeV provides neutrons up to 3.2 MeV but none at higher energies, since it is a threshold reaction. The required peak proton current to achieve  $10^5$  counts/s is 2.5 mA, compared to a peak current of 1.9 mA for the  $\text{Be}(\text{d},\text{n})$  source with  $E_d = 4.2$  MeV.

Flight path length is another important system parameter. Shorter flight paths make the system footprint smaller, but decrease resolution and increase potential scattering problems. Transmission simulations were performed using the  $^9\text{Be}(\text{d},\text{n})$  source with  $E_d = 4.2$  MeV and flight paths of five, three, and two meters. The transmission results were unfolded using cross sections calculated separately for each path length. The resulting three-angle reconstructions are shown in Figure 4. For the five- and three-meter cases, the explosive is clearly visible, although the equivalent explosive density is less for the three-meter flight path. At two meters, the explosive is still visible, but at still lower density. The contribution of scattered neutrons for shorter flight paths makes the transmission appear higher, and thus the amount of material appear lower.

Placement of the sample nearer to the detector array would reduce the size of the array, but again at the price of an increase in scattered neutrons detected. Simulations of fan-beam irradiation for a five-meter flight path with  $E_d = 5$  MeV and for a three-meter flight path with  $E_d = 4.2$  MeV show that accurate unfolding results can be obtained when the sample is at least one meter from the detector array. For a sample-detector distance of 50 cm, errors in unfolding are somewhat larger (10%) for very thick or very thin samples (transmissions much less or much greater than used for the cross section determination), but still consistent with statistical variations in the results.

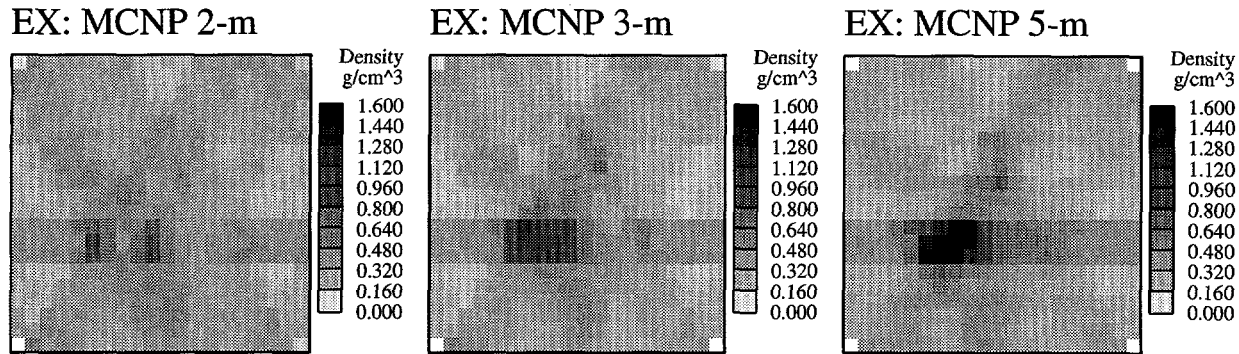


Figure 4. Change in explosive signature as a function of the neutron flight path.

## 7. Conclusions

We have developed a model of a few-angle tomographic FNTS system that allows system performance to be easily determined as various system designs, algorithms, and parameters are varied. Our element unfolding algorithms have been tested with both MCNP-simulated transmission data and actual experimental neutron transmission data and there is good agreement between the actual areal densities and the unfolded results. We have shown that tomographic reconstruction combined with simple explosive detection and image processing algorithms can detect explosives using exact projection data and Monte Carlo derived transmission data. Application of the unfolding, reconstruction, explosive detection and image processing algorithms to reconstruction of suitcase slices for which few-view transmission data were acquired experimentally shows that the location and the shape of bulk explosives can be readily determined. We have modeled the FNTS system performance using ROC curves and a random suitcase packing algorithm. These ROC studies show that it is relatively easy to detect bulk explosives with FNTS and a few projection angles, but that detection of thin slabs will be considerably more difficult.

## Acknowledgments

This work was supported by the U.S. Federal Aviation Administration Technical Center under contract DTFA03-93-X-00021. Prof. J. C. Overley at the University of Oregon provided the experimental neutron transmission data.

## 8. REFERENCES

1. B. J. Micklich, C. L. Fink, L. Sagalovsky, D. L. Smith, and T. J. Yule, FAA Technical Report, DOT/FAA/CT-95/XX (December, 1995).
2. J. A. Swets, *Science*, 132, 990-1000 (Dec. 1973).
3. J. C. Overley, *J. Appl. Radiat. Isot.* **36**, 185-191 (1985); *Nucl. Instr. Meth.* **B24/25**, 1058-1062 (1987).
4. B. J. Micklich, M. K. Harper, A. H. Novick, and D. L. Smith, *Nucl. Instr. Meth.* **A353**, 646-649 (1994).
5. C. L. Fink, B. J. Micklich, T. J. Yule, P. Humm, L. Sagalovsky, and M. M. Martin, *Nucl. Instr. Meth.* **B99**, 748-752 (1996).
6. J. Briesemeister, ed., LA-12625-M, Los Alamos National Laboratory (Nov. 1993).
7. T. J. Yule, B. J. Micklich, C. L. Fink, and L. Sagalovsky, 5<sup>th</sup> International Conference on Applications of Nuclear Techniques, "Neutrons in Research and Industry, Crete, Greece (June 9-15, 1996).
8. J. C. Overley, M. S. Chmelik, R. J. Rasmussen, R. M. S. Schofield, and H. W. Lefevre, DOT/FAA/CT-94/103 (Aug. 1994).
9. B. J. Micklich, M. K. Harper, L. Sagalovsky, and D. L. Smith, Proc. International Conference on Nuclear Data for Science and Technology, Gatlinburg, TN (May 1994).
10. C. L. Fink, P. G. Humm, M. M. Martin, and B. J. Micklich, *IEEE Trans. on Nuclear Science*, **43**, 1352-1356 (June 1996).
11. B. J. Micklich, C. L. Fink, and L. Sagalovsky, European Symposium on Optics for Environmental and Public Safety, SPIE **2511**, 33-44, Munich, Germany (June 1995).
12. P. G. Humm, Master of Science Thesis in Nuclear Engineering, University of Illinois (1996).